Electronic Structure, Surface Doping, and Optical Response in Epitaxial WSe₂ Thin Films

Yi Zhang,[*,†,‡,§] Miguel M. Ugeda,[∥,⊥,#] Chenhao Jin,[∥] Su-Fei Shi,[∥,∇] Aaron J. Bradley,[∥] Ana Martín-Recio,[∥,○] Hyejin Ryu,[§,◆] Jonghwan Kim,[∥] Shujie Tang,[¶,□] Yeongkwan Kim,[§] Bo Zhou,[§,¶,■] Choongyu Hwang,[◆,●] Yulin Chen,[■] Feng Wang,[∥,▲,⬡] Michael F. Crommie,[∥,▲,○] Zahid Hussain,[§] Zhi-Xun Shen,[‡,¶] and Sung-Kwan Mo[*,§]

[†]National Laboratory of Solid State Microstructures, School of Physics, Collaborative Innovation Center of Advanced Microstructures, Nanjing University, Nanjing 210093, China

[‡]Stanford Institute of Materials and Energy Sciences, SLAC National Accelerator Laboratory, Menlo Park, California 94025, United States

[§]Advanced Light Source, Lawrence Berkeley National Laboratory, Berkeley, California 94720, United States

[∥]Department of Physics, University of California at Berkeley, Berkeley, California 94720, United States

[⊥]CIC nanoGUNE, 20018 Donostia-San Sebastian, Spain

[#]Ikerbasque, Basque Foundation for Science, 48011 Bilbao, Spain

[∇]Department of Chemical and Biological Engineering, Rensselaer Polytechnic Institute, Troy, New York 12180, United States

[○]Departamento de Física de la Materia Condensada, Universidad Autónoma de Madrid, E-28049 Madrid, Spain

[◆]Max Plank POSTECH Center for Complex Phase Materials, Pohang University of Science and Technology, Pohang 790-784, Korea

[¶]Geballe Laboratory for Advanced Materials, Departments of Physics and Applied Physics, Stanford University, Stanford, California 94305, United States

[□]State Key Laboratory of Functional Materials for Informatics, Shanghai Institute of Microsystem and Information Technology, Chinese Academy of Sciences, Shanghai 200050, China

[■]Department of Physics and Clarendon Laboratory, University of Oxford, Parks Road, Oxford, OX1 3PU, United Kingdom

[●]Department of Physics, Pusan National University, Busan 609-735, Korea

[▲]Materials Sciences Division, Lawrence Berkeley National Laboratory, Berkeley, California 94720, United States

[⬡]Kavli Energy NanoScience Institute at the University of California Berkeley and the Lawrence Berkeley National Laboratory, Berkeley, California 94720, United States

ⓈSupportingInformation

ABSTRACT: High quality WSe₂ films have been grown on bilayer graphene (BLG) with layer-by-layer control of thickness using molecular beam epitaxy. The combination of angle-resolved photoemission, scanning tunneling microscopy/spectroscopy, and optical absorption measurements reveal the atomic and electronic structures evolution and optical response of WSe₂/BLG. We observe that a bilayer of WSe₂ is a direct bandgap semiconductor, when integrated in a BLG-based heterostructure, thus shifting the direct−indirect band gap crossover to trilayer WSe₂. In the monolayer limit, WSe₂ shows a spin-splitting of 475 meV in the valence band at the K point, the largest value observed among all the MX₂ (M = Mo, W; X = S, Se) materials. The exciton binding energy of monolayer-WSe₂/BLG is found to be 0.21 eV, a value that is orders of magnitude larger than that of conventional three-dimensional semiconductors, yet small as compared to other two-dimensional transition metal dichalcogennides (TMDCs) semiconductors. Finally, our finding regarding the overall modification of the electronic structure by an alkali metal surface electron doping opens a route to further control the electronic properties of TMDCs.

KEYWORDS: Transition metal dichalcogenides, WSe₂, MBE, ARPES, STM/STS, exciton binding energy
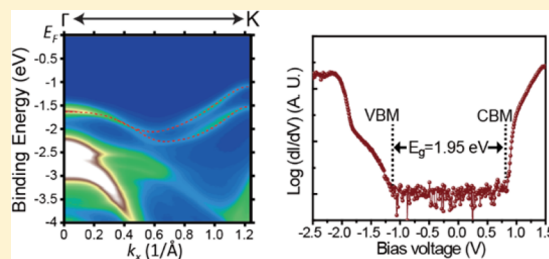
Two-dimensional (2D) transition metal dichalcogenides (TMDCs) MX$_2$ (M = Mo, W; X = S, Se) semiconductors have attracted extensive interest due to their remarkable fundamental properties distinct from those of their bulk counterparts.[1−4] These include direct electronic bandgap in the single-layer limit,[5−10] spin-splitting of the valence band (VB),[11−15] a well-pronounced valley degree of freedom[16−20] as well as the excitonic nature of their optical spectra.[20−24] Large efforts are currently devoted to tailor these properties in order to widen further the versatility of these materials and to achieve practical devices out of them.[25−38] Some proposed strategies in these regards are the growth of films with varying thickness,[14,39−42] their growth on other 2D materials to form hybrid heterostructures,[28,31,35,37,43] and the use of chemical and electrostatic doping.[13,29,44−46] All of them have been demonstrated to be very successful in modifying and controlling the properties of graphene, which have even led to the observation of novel physical phenomena.[47−51] Nonetheless, these strategies have been less explored in TMDC materials although promising results have recently been predicted.[37]

Among the family of TMDC semiconductors, WSe$_2$ is probably the most interesting material for potential applications. It is expected to possess the largest spin-splitting in the VB at the K/K′ point among all the MX$_2$ semiconductors,[11] which makes WSe$_2$ an ideal platform for studying spin and valley dependent properties as well as for spintronic applications.[18,44] The recent polarization dependent photoluminescence (PL) indicates that the valley coherence is preserved for longer time compared to other TMDCs,[52] which makes WSe$_2$ a more promising candidate for valleytronics. So far, detailed spectroscopic research on the electronic structure of monolayer WSe$_2$ is rather scarce due to the difficulty in obtaining high-quality thin films and hybrid heterostructures with uniform thickness,[53] which to date can be only obtained via chemical vapor deposition[42] and in a lesser extent via molecular beam epitaxy (MBE).[8]

Here we report the MBE growth and subsequent characterization of hybrid heterostructures formed by high-quality one-atomic-plane precision films of WSe$_2$ with varying thicknesses from 1−8 monolayers (MLs) on a bilayer graphene (BLG) substrate. Combining in situ angle-resolved photoemission spectroscopy (ARPES), optical absorption, scanning tunneling microscopy/spectroscopy (STM/STS), core level spectroscopy, low energy electron diffraction (LEED) and reflection high-energy electron diffraction (RHEED) techniques, we study the atomic and electronic structures evolution and optical response of these heterostructures. Remarkably, we find that a bilayer of WSe$_2$ remains a direct bandgap semiconductor when it is part of a BLG-based heterostructure, thus shifting the direct−indirect bandgap crossover to the trilayer of WSe$_2$. Furthermore, our ARPES spectra show a rather large spin-splitting of 475 meV in the VB at the K points of the Brillouin zone of the 1 ML WSe$_2$/BLG heterostructure. We also present an unambiguous experimental measurement of the binding energy for neutral excitons in this heterostructure. We obtain an exciton binding energy of 0.21 eV for this TMDC semiconductor on BLG, a value that is orders of magnitude larger than that was observed in conventional 3D semiconductors and yet is intriguingly smaller as compared to other TMDCs.[22−24] Lastly, we analyze the evolution of the size and the character of the electronic band gap with chemical surface doping. Overall, our results provide a well-defined route to create high-quality large-scale WSe$_2$/BLG heterostructures as well as new avenues to tailor the electronic and optoelectronic properties of TMDCs.

Figure 1a−c shows the crystal structure of WSe$_2$. A single layer (Se−W−Se) of WSe$_2$ consists of two planes of Se atoms separated by one layer of W atoms in a trigonal prismatic coordination. Layers of WSe$_2$ are vertically stacked by van der Waals interactions in an AB configuration. Figure 1d shows the 2D Brillouin zone of the WSe$_2$ layers. Because the bandgap of MX$_2$ semiconductors is along the Γ K direction, we will focus on this direction in the following ARPES measurements. BLG is an ideal substrate for epitaxial growth of layered materials such as Bi$_2$Se$_3$ and MoSe$_2$ due to its honeycomb atomic structure and van der Waals nature.[8,40,54] An important advantage of BLG substrate for high-quality growth is that the lattice constant ratio between BLG and WSe$_2$ is very close to 3:4,[7] which facilitates WSe$_2$ to form a single-crystalline thin film. To prepare an uniform BLG substrate, a *6H*-SiC(0001) wafer was first initially degassed at 650 °C in the ultrahigh vacuum (UHV) chamber for 3 h, followed by 80 cycles of flash-annealing to 1300 °C.[55] Figure 1e,h shows the RHEED and LEED patterns of BLG substrate, respectively. The characteristic sharp diffraction patterns of graphene indicate the high quality of the substrate. For the growth of WSe$_2$ thin film, high-purity W and Se were evaporated from an electron-beam evaporator and a standard Knudsen cell, respectively. The flux ratio of W/Se was controlled to be ∼1:30. Excess amount of Se was deposited to avoid Se vacancy and W cluster nucleation in the film. The BLG substrate was kept at ∼400 °C during the growth. This substrate temperature leads a stoichiometric crystallization of WSe$_2$ film. After growth, we postannealed the film at ∼550 °C under Se flux for 10 min to improve the crystalline quality. The film thickness was accurately controlled by the deposition time with a growth rate of 17 min per monolayer, monitored by the in situ RHEED. Afterward, its crystal orientation and quality was also checked by in situ LEED.

Figure 1f,i shows the RHEED and LEED patterns of the WSe$_2$ film for a coverage of 0.7 ML (0.7 ML means that a 70% area of the substrate surface was covered by monolayer WSe$_2$), respectively. In these patterns, both the BLG and WSe$_2$ diffraction spots can be observed. The LEED pattern shows the diffraction spots of WSe$_2$ aligned with those of the BLG substrate although slightly stretched along the rotational direction. This reveals that the first layer of WSe$_2$ has the same atomic lattice orientation as the BLG substrate although it also presents domains with small rotational misorientation ($\theta < \pm 4°$). When the coverage reached 1 ML, the RHEED pattern of BLG vanishes (Figure 1g) and only the WSe$_2$ pattern can be observed. In the corresponding LEED pattern (Figure 1j), the pattern of BLG is barely visible and much weaker than that of the WSe$_2$.

We also performed core level spectroscopy and low temperature (5 K) STM measurements for a thorough characterization of the atomic structure of the WSe$_2$ films. Figure 1k shows a typical angle-integrated core level spectrum taken by the in situ ARPES system. The sharp characteristic peaks of Se (54.7 eV of 3d5/2 orbit and 55.5 eV of 3d3/2 orbit) and W (32.5 eV of 4f7/2 orbit, 34.6 eV of 4f5/2 orbit and 37.9 eV of 5p3/2 orbit) indicate the 2:1 stoichiometry and demonstrate the purity of the WSe$_2$ films. The atomically resolved STM image of monolayer WSe$_2$ on BLG (Figure 1l) shows simultaneously an atomic periodicity of 3.29 Å and a moiré pattern formed between the graphene and the WSe$_2$ atomic lattices. Similar to the epitaxial MoSe$_2$ on BLG/SiC(0001), the moiré pattern in 1-ML-WSe$_2$/BLG is a (3 × 3) structure with respect to WSe$_2$ with a periodicity between 9.9 to 9.3 Å,[23] which confirms the aligned orientation of the WSe$_2$/BLG heterostructure deduced from LEED patterns (Figure 1i,j).
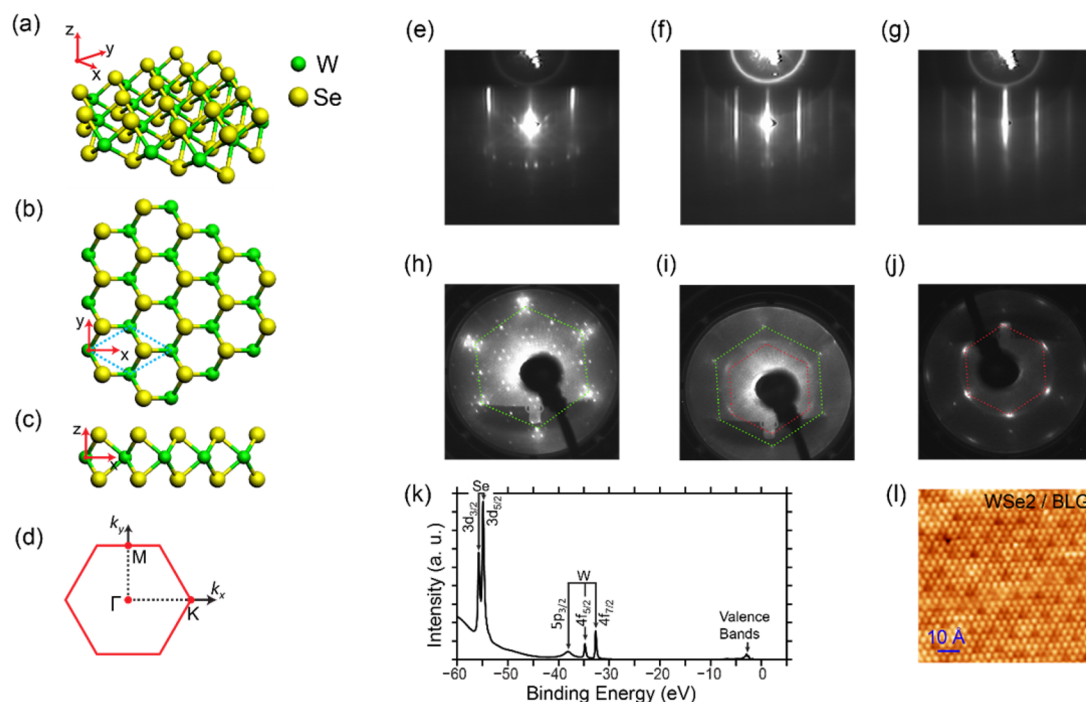
Figure 1. Growth of WSe_2 thin films. (a−c) Crystal structure of 2D WSe_2 with (a) perspective view, (b) top view, and (c) side view, respectively. (d) The 2D Brillouin zone of WSe_2 film. (e−g) RHEED pattern along the Γ K direction of (e) BLG substrate, (f) 0.7 ML WSe_2 film, and (g) monolayer WSe_2 film, respectively. (h−j) LEED pattern of (h) BLG substrate, (i) 0.7 ML WSe_2 film, and (j) monolayer WSe_2 film, respectively. The dotted green and red hexagon indicates 1×1 diffraction pattern of BLG substrate and epitaxial WSe_2 film, respectively. (k) Core-level spectrum of epitaxial WSe_2 film. (l) STM image of WSe_2 film ($V_s = -1.3$ V, $I_t = 0.6$ nA, $T = 5$ K).

For a systematic characterization of the electronic properties of variable-thickness WSe_2/BLG heterostructures, we first explored their band structure by performing in situ ARPES measurements. Figure 2a−d presents the ARPES spectra of the epitaxial WSe_2 thin films along the Γ K direction with varying film thicknesses of 1, 2, 3, and 8 ML. Figure 2e−h shows the corresponding second-derivatives of the original spectra in Figure 2a-d for enhanced visibility of the band structures. The contribution from BLG is out of this momentum window (Supporting Information A). The top of the VBs, depicted by red dashed lines in Figure 2a−d, shows a different number of the branches at the Γ point following the number of layers; for monolayer WSe_2, the Γ point shows only one branch at the top of the VB. It splits into two branches for 2 ML, and then into three branches in the 3 ML film. For the 8 ML WSe_2 film, theory suggests eight branches to appear,[7] but we can only observe broadened multiple bands due to the limited resolution and narrower spacing of branches in energy. Because the number of branches in the VB near the Γ point corresponds to the number of layers, this can be used as unique identifier of the thickness of the ultrathin WSe_2 films.

To gain further information on the VB evolution with varying film thickness, we present zoom-in ARPES spectra focusing only on the top of the VB in Figure 2i−l. The most important feature in the evolution of the band structure of MX_2 semiconductors is the indirect to direct bandgap transition. This bandgap transition is concomitant with the change of the valence band maximum (VBM) from the Γ point to the K point in the monolayer limit as predicted in theoretical calculations[7] and observed in previous ARPES measurements for $MoSe_2$ and MoS_2.[8,9] Our ARPES spectra on monolayer WSe_2 show that the VBM is located at the K point and 0.56 ± 0.01 eV higher than the top of the VB at the Γ point. The precise energy positions of each band were assigned from a fitting using multiple Gaussian peaks for the energy

distribution curves (EDCs) at the Γ and K points (Supporting Information B). The energy difference between the K and Γ points in the VB ($E_K - E_\Gamma = 0.56$ eV) for monolayer WSe_2 is significantly larger than that of monolayer $MoSe_2$ (0.38 eV)[8] and MoS_2 (0.31 eV).[14] The larger difference ($E_K - E_\Gamma$) implies the strongest tendency of monolayer WSe_2 to maintain a direct bandgap among all the MX_2 (M = Mo, W and X = S, Se) semiconductors.[7] The transition to an indirect bandgap has clearly been observed in 2 ML $MoSe_2$ and MoS_2.[8,9] In contrast, our ARPES spectra show that the top of VB at the K point is still 0.08 eV higher than that at the Γ point for 2 ML WSe_2 on BLG, thus enabling the possibility that the 2 ML WSe_2 in the heterostructure may be a direct bandgap semiconductor. For 3 and 8 ML WSe_2, the top of the VB at the Γ point is slightly higher than that at the K point and becomes the VBM, which suggests that the direct to indirect bandgap transition may occur between 2 and 3 ML in WSe_2.

Another key property of MX_2 semiconductors is the spin-split band structure due to strong spin−orbit coupling and inversion symmetry breaking.[11] Monolayer WSe_2 has been theoretically predicted to have the largest splitting size among all the MX_2 semiconductors.[11] As shown in the ARPES spectra of Figure 2i, the VB at the K point splits into two branches separated by 475 ± 5 meV, which is much larger than that measured for monolayer $MoSe_2$ (∼180 meV, ref 8) and MoS_2 (∼150 meV, ref 14). This is due to the largely enhanced spin−orbit coupling in W as compared to that in Mo and makes WSe_2 particularly promising among all the TMDC compounds for spintronic applications.

To evaluate the bandgap character, direct or indirect, of the WSe_2 films on BLG, we study the conduction band minimum (CBM) location in energy and momentum by controlled surface doping of the WSe_2 with alkali metal (Na and K) at 60 K (Supporting Information C). This procedure allows us to shift
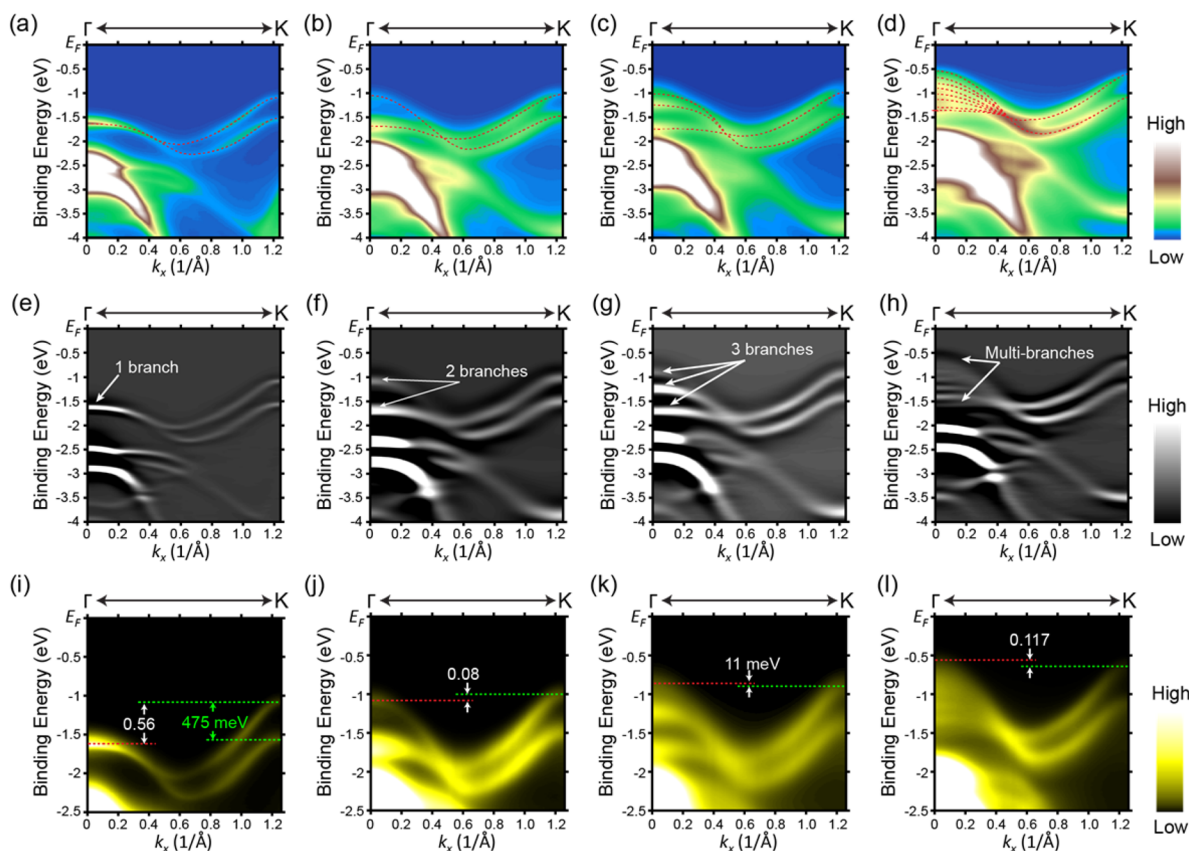
Figure 2. ARPES data of epitaxial WSe$_2$ thin films. (a−d) ARPES spectra of (a) 1, (b) 2, (c) 3, and (d) 8 ML WSe$_2$ films along the Γ K direction. The red-dotted curves depict the top VBs. (e−h) Second-derivative ARPES spectra of (e) 1, (f) 2, (g) 3, and (h) 8 ML WSe$_2$ films along the Γ K direction. (i,j) Zoom-in ARPES spectra of (i) 1, (j) 2, (k) 3, and (l) 8 ML WSe$_2$ films along the Γ K direction. The red and green dotted lines indicate the energy positions of top of VB at the Γ and K point, respectively. All the labeled numbers have units of electronvolts.

the Fermi level (E_F) upward to make the CBM accessible for ARPES.[56] Although we have used both Na and K adatoms to this purpose, only K doping enabled us to shift the CBM below E_F. ARPES spectra of K-doped monolayer WSe$_2$ on BLG (Figure 3a) reveals that the CBM becomes visible at the K point, as expected for a single layer of a MX$_2$ semiconductors, and the VB shifts downward 0.56 and 0.47 eV at the Γ and K point, respectively. Therefore, the monolayer K-doped WSe$_2$ shows a direct electronic bandgap of 1.40 ± 0.02 eV. In the ARPES spectrum for K-doped 2 ML-WSe$_2$ (Figure 3b), while the CBM remains at the K point, the VBM now shifts to the Γ point, which leads to an indirect bandgap of 1.26 eV. Similar energetics have been observed for the K-doped 8 ML WSe$_2$ (Figure 3c), which shows an indirect bandgap of 1.01 eV. These gap values are much smaller than that expected for single- and few-layer MX$_2$ semiconductors and even for MX$_2$/BLG heterostructures (refs 23 and 57). This is caused by a doping-induced enhancement of charge screening at the semiconductor, which leads to the band structure renormalization.[45]

In contrast with our experimental results, previous calculations have shown that the CBM of isolated WSe$_2$ from 2 ML to bulk is located at the midpoint between the Γ and K point (Q point).[7,10] This discrepancy can be attributed to the strain effect induced by the BLG substrate due to the lattice mismatch between the film and the substrate.[58] This affects the momentum location of CBM, the energy difference between the K and Γ point in the VB ($E_K − E_Γ$), as well as the splitting at the K point.[26,32,33] Furthermore, the difference in energy of the VB between the K and Γ points ($E_K − E_Γ = 0.56$ eV) and the energy splitting at the
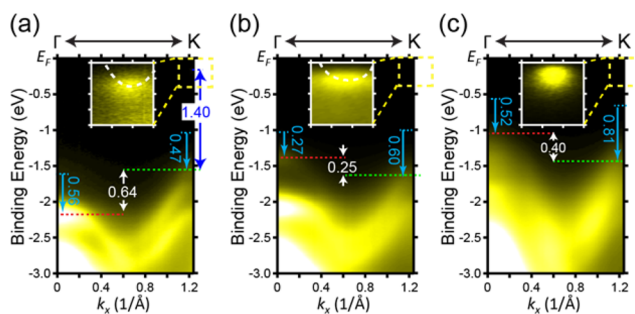
Figure 3. Surface doping effect of WSe$_2$ films. (a−c) ARPES spectra of (a) 1 ML, (b) 2 ML and (c) 8 ML WSe$_2$ films with K surface doping. The red and green dotted lines indicate the energy positions of top of VB at the Γ and K point, respectively. Cyan arrows and numbers show the band movements at the Γ and K point after surface doping comparing to undoped films. Insets in (a−c) are the zoom-in spectra with 10 times enhanced intensity to make the CBM visible. All the labeled numbers have unit of electronvolts.

K point (475 meV) in monolayer WSe$_2$ are both smaller than those found for the exfoliated WSe$_2$ (0.89 eV and 513 meV),[53] which is also suggestive of strain induced in WSe$_2$ by the BLG in the heterostructure.

Our ARPES measurements on K-doped WSe$_2$/BLG reveal that the CBM remains at the K point from 1 ML up to 8 ML of WSe$_2$. Combining this observation with our ARPES spectra on VBs of pristine WSe$_2$ films, we suggest that the direct−indirect bandgap transition occurs from 2 to 3 ML for undoped WSe$_2$

epitaxial films on BLG. Because the energy difference between the VBs at Γ and K points is small ($E_\Gamma - E_K \sim 0.01$ eV) for 2 and 3 ML WSe_2, and the in-plane strain could also renormalize the VB of MX_2 semiconductors, the crossover thickness of the direct−indirect bandgap transition could be engineered by strain. For the surface doping effect, the momentum position inversion in VBM for K-surface-doped 2 ML WSe_2 implies a new method to control the direct−indirect bandgap transition via surface chemical doping. These observations paint a clear picture of the effect of chemical doping and strain on the electronic structure of thin films of MX_2 semiconductors integrated in hybrid heterostructures.

Because of the changes introduced in the band structure in surface-doped thin films, ARPES is not an accurate tool to measure the quasiparticle bandgap of pristine TMDCs. In order to investigate the fundamental optical and electronic bandgaps of pristine WSe_2, we performed both optical absorbance and high-resolution STS on our epitaxial monolayer WSe_2 thin films. This combined experimental approach also allows us to obtain an accurate and unambiguous value for the exciton binding energy, a critical parameter for understanding how light interacts with TMDC materials, in particular regarding processes such as its optical absorption and photovoltaic response.

Figure 4a shows the optical absorbance spectrum of the monolayer WSe_2 film taken at 77 K. The A exciton peak is broad,
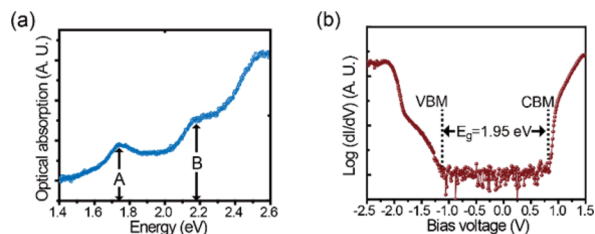
Figure 4. Optical and electronic bandgap of epitaxial monolayer WSe_2. (a) Optical absorption spectrum taken on monolayer WSe_2 film. The two main absorption peaks A and B are indicated. (b) STS spectrum taken on monolayer WSe_2 film (f = 871 Hz, I_t = 50 nA, V_{rms} = 1.5 mV, T = 5 K).

likely due to charge transfer and energy transfer between the WSe_2 and the graphene, but clearly resolved with the center at 1.74 ± 0.01 eV (713 nm). This is consistent with previous reports on exfoliated WSe_2 monolayers.[59] The absorption signal around the B exciton peak is even broader and centered around 2.17 eV ($\sim$570 nm). The energy difference between the two absorption peaks ($\sim$0.43 eV) agrees with the band splitting energy observed in the ARPES spectra in Figure 2i. The absorption spectrum at room temperature is also provided in Supporting Information D. Measurement of the electronic bandgap (E_g) of undoped single-layer WSe_2 was performed by STS at T = 5 K. Typical STS dI/dV spectrum acquired on monolayer WSe_2 exhibits large electronic bandgap (E_g) around E_F, as shown in Figure 4b. The locations of the VBM and the CBM and, therefore, the value of E_g were obtained by means of statistical analysis using a sample of N = 30 dI/dV curves and following the fitting procedure detailed in ref 23. VBM in monolayer WSe_2 is found to be located at -1.10 ± 0.02 V, which nicely agrees with our ARPES result, and the CBM at $+0.85 \pm 0.03$ V. The asymmetry of the VBM and CBM respect to E_F reveals a slight n-type doping of our WSe_2 films, albeit with a negligible carrier concentration. The nearly intrinsic character of our epitaxial WSe_2 films suggests a high

crystal quality, which is in accordance with the low concentration of point defects found from our STM images (Supporting Information E), which are known to be a source of doping in TMDC materials.[30] Our statistical analysis of the STS spectra yields a value for the single-particle electronic bandgap of $E_g = E_{CBM} - E_{VBM} = 1.95 \pm 0.04$ eV. For a direct bandgap semiconductor such as monolayer WSe_2, the difference between the electronic bandgap and the optical bandgap represents the exciton binding energy (E_b), which in the present case we have found to be $E_b = E_g - E_{opt} = 0.21 \pm 0.04$ eV.

This large exciton binding energy is explained by enhanced Coulomb interactions in low-dimensional systems.[20−23] The large dielectric constant in bulk semiconductors gives rise to reduced strength of the Coulomb interaction and, therefore, limits the binding energies of these excitations within few millielectronvolts. In 2D systems, reduced screening leads to enhanced Coulomb interactions, which significantly increase the binding energy of electron−hole excitations.[22] We have recently demonstrated these effects for 2D TMDC and reported an exciton binding energy of 0.55 eV for single layer of epitaxial $MoSe_2$ film on BLG.[23] Using this method, we have been able to extract a large exciton binding energy of 0.21 eV for epitaxially grown monolayer WSe_2 on BLG, that is, however, significantly smaller than that of monolayer $MoSe_2$ film.[23] These results are smaller than the exciton binding energy of single-layer WSe_2 on insulating environments such as SiO_2 estimated by optical methods, which ranges from 0.37[59] up to 0.6 eV,[60] likely due to the increased screening substrate (BLG) environment.

This exciton binding energy is several times larger than those extracted for bulk TMDCs[22] and therefore demonstrates the enhanced coulomb interactions in the monolayer limit for WSe_2. However, this value is 62% smaller than that measured for monolayer $MoSe_2$ on the same substrate.[23] The smaller exciton binding energy is caused by both a larger electronic gap and smaller optical bandgap than those found in $MoSe_2$. Therefore, this difference is not caused by the dielectric environment but has its origin in the distinct metal atom between the two compounds. It is worth noting that a similar binding energy has been reported on WSe_2 on SiO_2 substrate.[59] This drastic difference in the exciton binding energy among the different TMDCs is very intriguing itself and calls for further theoretical attention.

Interestingly, the electronic bandgap measured in ARPES (1.40 ± 0.02 eV) is significantly smaller than that measured by STS (1.95 ± 0.04 eV). The different values of the bandgap measured by ARPES and STS are due to the surface doping. While the STS bandgap was measured on undoped thin films, the bandgap measurement by ARPES was performed on the K-doped films. We suggest the K surface doping induces a bandgap renormalization due to extra free carriers on the film, which effectively increases charge screening in the material. This naturally reduces both the quasiparticle bandgap and the exciton binding energy. As it has been previously shown in Na-doped MoS_2, alkali metal surface doping on MX_2 reduces the bandgap by mainly affecting the CB rather than the VB.[45]

In conclusion, we successfully synthesized ultrathin WSe_2 film on epitaxial BLG substrate with controllable thickness at the atomic level. In situ ARPES measurements directly demonstrate the layer-by-layer electronic structure evolution of the epitaxial WSe_2 film, suggesting a direct bandgap in monolayer and 2 ML WSe_2 and indirect bandgap for 3 or more ML WSe_2 on BLG substrate. In monolayer WSe_2 film, we also observed a giant VB splitting (475 ± 5 meV) at the K point, which is larger than any other monolayer of MX_2. The further surface doping

experiments show that the electronic structure undergoes a significant change, allowing us a further control of band structure of WSe$_2$, such as the size of the gap and direct−indirect bandgap transition. The exciton binding energy observed in monolayer WSe$_2$ highlights the importance of many-body effects in atomically thin 2D layers and has a profound impact on future technologies involving single-layer semiconducting TMDCs, such as solar cells and valleytronic devices, either in stand-alone devices or within integrated heterostructures. Our MBE growth of WSe$_2$ and studies on the VB evolution, VB splitting at K point, surface doping effect, bandgap, and excitonic effect not only help understanding of TMDC materials but also enrich the family of epitaxial 2D materials toward a fully MBE grown epitaxial heterostructures for light emission and photon-voltage devices.[4,37]

Experimental Section. The growth of WSe$_2$ thin film and in situ ARPES measurements were performed at the HERS endstation of beamline 10.0.1, Advanced Light Source, Lawrence Berkeley National Laboratory. The base pressures for the MBE system and ARPES system were $\sim 2 \times 10^{-10}$ and $\sim 4 \times 10^{-11}$ Torr, respectively. ARPES data were taken with a Scienta R4000 electron analyzer at a temperature of 60 K. The photon energy was set at 70 eV with an energy and an angular resolution of 15 meV and 0.1°, respectively. The photon polarization direction was set to be 78° out of the incidence plane for an evenly distributed even and odd state signal. The size of the beam spot on the sample was $\sim 150 \ \mu m \times 200 \ \mu m$. To protect the WSe$_2$ films from contamination of air during its transfer to the UHV-STM system, an ~ 100 Å amorphous Se capping layer was deposited on the sample before moving it out of the UHV-MBE chamber. Further annealing at ~ 300 °C for 1 h in the UHV-STM system was enough to remove the Se capping layer and uncover the pristine WSe$_2$ surface. Optical absorbance measurements were taken with a reflection configuration of a confocal microscope setup, using supercontinuum white laser as the light source (focus spot $\sim 2 \ \mu m$).

ASSOCIATED CONTENT

Ⓢ Supporting Information

The Supporting Information is available free of charge on the ACS Publications website at DOI: 10.1021/acs.nanolett.6b00059.

Contribution of BLG band from the WSe$_2$ film in ARPES spectra, multiple Gaussian peaks fitting of the EDCs in ARPES spectra, the detailed surface doping effect in MX$_2$ films, optical absorption spectrum at different temperature, density of defects in WSe$_2$ films. (PDF)

AUTHOR INFORMATION

Corresponding Authors

*E-mail: zhangyi@nju.edu.cn.

*E-mail: skmo@lbl.gov.

Notes

The authors declare no competing financial interest.

ACKNOWLEDGMENTS

REFERENCES

(1) Balendhran, S.; Walia, S.; Nili, H.; Ou, J. Z.; Zhuiykov, S.; Kaner, R. B.; Sriram, S.; Bhaskaran, M.; Kalantar-zadeh, K. *Adv. Funct. Mater.* **2013**, *23*, 3952−3970.

(2) Butler, S. Z.; Hollen, S. M.; Cao, L.; Cui, Y.; Gupta, J. A.; Gutiérrez, H. R.; Heinz, T. F.; Hong, S. S.; Huang, J.; Ismach, A. F.; Johnston-Halperin, E.; Kuno, M.; Plashnitsa, V. V.; Robinson, R. D.; Ruoff, R. S.; Salahuddin, S.; Shan, J.; Shi, L.; Spencer, M. G.; Terrones, M.; Windl, W.; Goldberger, J. E. *ACS Nano* **2013**, *7* (4), 2898−2926.

(3) Tan, C.; Zhang, H. *Chem. Soc. Rev.* **2015**, *44* (9), 2713−2731.

(4) Xia, F.; Wang, H.; Xiao, D.; Dubey, M.; Ramasubramaniam, A. *Nat. Photonics* **2014**, *8* (12), 899−907.

(5) Splendiani, A.; Sun, L.; Zhang, Y.; Li, T.; Kim, J.; Chim, C.-Y.; Galli, G.; Wang, F. *Nano Lett.* **2010**, *10* (4), 1271−1275.

(6) Ellis, J. K.; Lucero, M. J.; Scuseria, G. E. *Appl. Phys. Lett.* **2011**, *99* (26), 261908.

(7) Kumar, A.; Ahluwalia, P. K. *Eur. Phys. J. B* **2012**, *85* (6), 186.

(8) Zhang, Y.; Chang, T.-R.; Zhou, B.; Cui, Y.-T.; Yan, H.; Liu, Z.; Schmitt, F.; Lee, J.; Moore, R.; Chen, Y.; Lin, H.; Jeng, H.-T.; Mo, S.-K.; Hussain, Z.; Bansil, A.; Shen, Z.-X. *Nat. Nanotechnol.* **2013**, *9* (2), 111−115.

(9) Jin, W.; Yeh, P.-C.; Zaki, N.; Zhang, D.; Sadowski, J. T.; Al-Mahboob, A.; van der Zande, A. M.; Chenet, D. A.; Dadap, J. I.; Herman, I. P.; Sutter, P.; Hone, J.; Osgood, R. M. *Phys. Rev. Lett.* **2013**, *111* (10), 106801.

(10) Roldán, R.; Silva-Guillén, J. A.; López-Sancho, M. P.; Guinea, F.; Cappelluti, E.; Ordejón, P. *Ann. Phys.* **2014**, *526* (9−10), 347−357.

(11) Zhu, Z. Y.; Cheng, Y. C.; Schwingenschlögl, U. *Phys. Rev. B: Condens. Matter Mater. Phys.* **2011**, *84* (15), 153402.

(12) Sun, L.; Yan, J.; Zhan, D.; Liu, L.; Hu, H.; Li, H.; Tay, B. K.; Kuo, J.-L.; Huang, C.-C.; Hewak, D. W.; Lee, P. S.; Shen, Z. X. *Phys. Rev. Lett.* **2013**, *111* (12), 126801.

(13) Alidoust, N.; Bian, G.; Xu, S. Y.; Sankar, R.; Neupane, M.; Liu, C.; Belopolski, I.; Qu, D. X.; Denlinger, J. D.; Chou, F. C.; Hasan, M. Z. *Nat. Commun.* **2014**, *5*, 4673.

(14) Miwa, J. A.; Ulstrup, S.; Sørensen, S. G.; Dendzik, M.; Čabo, A. G.; Bianchi, M.; Lauritsen, J. V.; Hofmann, P. *Phys. Rev. Lett.* **2015**, *114* (4), 046802.

(15) Riley, J. M.; Mazzola, F.; Dendzik, M.; Michiardi, M.; Takayama, T.; Bawden, L.; Granerød, C.; Leandersson, M.; Balasubramanian, T.; Hoesch, M.; Kim, T. K.; Takagi, H.; Meevasana, W.; Hofmann, P.; Bahramy, M. S.; Wells, J. W.; King, P. D. C. *Nat. Phys.* **2014**, *10* (11), 835−839.

(16) Cao, T.; Wang, G.; Han, W.; Ye, H.; Zhu, C.; Shi, J.; Niu, Q.; Tan, P.; Wang, E.; Liu, B.; Feng, J. *Nat. Commun.* **2012**, *3*, 887.

(17) Mak, K. F.; He, K.; Shan, J.; Heinz, T. F. *Nat. Nanotechnol.* **2012**, *7* (8), 494−498.

(18) Xiao, D.; Liu, G.-B.; Feng, W.; Xu, X.; Yao, W. *Phys. Rev. Lett.* **2012**, *108* (19), 196802.

(19) Zeng, H.; Dai, J.; Yao, W.; Xiao, D.; Cui, X. *Nat. Nanotechnol.* **2012**, *7* (8), 490−493.

(20) Yu, H.; Cui, X.; Xu, X.; Yao, W. *National Science Review* **2015**, *2* (1), 57−70.

(21) Cheiwchanchamnangij, T.; Lambrecht, W. R. L. *Phys. Rev. B: Condens. Matter Mater. Phys.* **2012**, *85* (20), 205302.

(22) Komsa, H.-P.; Krasheninnikov, A. V. *Phys. Rev. B: Condens. Matter Mater. Phys.* **2012**, *86* (24), 241201.

(23) Ugeda, M. M.; Bradley, A. J.; Shi, S. F.; da Jornada, F. H.; Zhang, Y.; Qiu, D. Y.; Ruan, W.; Mo, S. K.; Hussain, Z.; Shen, Z. X.; Wang, F.; Louie, S. G.; Crommie, M. F. *Nat. Mater.* **2014**, *13* (12), 1091−5.

(24) Qiu, D. Y.; da Jornada, F. H.; Louie, S. G. *Phys. Rev. Lett.* **2013**, *111* (21), 216805.

(25) Yoon, Y.; Ganapathi, K.; Salahuddin, S. *Nano Lett.* **2011**, *11* (9), 3768−3773.

(26) Yun, W. S.; Han, S. W.; Hong, S. C.; Kim, I. G.; Lee, J. D. *Phys. Rev. B: Condens. Matter Mater. Phys.* **2012**, *85* (3), 033305.

(27) Yoon, J.; Park, W.; Bae, G.-Y.; Kim, Y.; Jang, H. S.; Hyun, Y.; Lim, S. K.; Kahng, Y. H.; Hong, W.-K.; Lee, B. H.; Ko, H. C. *Small* **2013**, *9* (19), 3185.

(28) Britnell, L.; Ribeiro, R. M.; Eckmann, A.; Jalil, R.; Belle, B. D.; Mishchenko, A.; Kim, Y.-J.; Gorbachev, R. V.; Georgiou, T.; Morozov, S. V.; Grigorenko, A. N.; Geim, A. K.; Casiraghi, C.; Neto, A. H. C.; Novoselov, K. S. *Science* **2013**, *340* (6138), 1311−1314.

(29) Das, S.; Chen, H.-Y.; Penumatcha, A. V.; Appenzeller, J. *Nano Lett.* **2013**, *13* (1), 100−105.

(30) Qiu, H.; Xu, T.; Wang, Z.; Ren, W.; Nan, H.; Ni, Z.; Chen, Q.; Yuan, S.; Miao, F.; Song, F.; Long, G.; Shi, Y.; Sun, L.; Wang, J.; Wang, X. *Nat. Commun.* **2013**, *4*, 2642.

(31) Terrones, H.; Lopez-Urias, F.; Terrones, M. *Sci. Rep.* **2013**, *3*, 1549.

(32) Amin, B.; Kaloni, T. P.; Schwingenschlögl, U. *RSC Adv.* **2014**, *4* (65), 34561.

(33) Desai, S. B.; Seol, G.; Kang, J. S.; Fang, H.; Battaglia, C.; Kapadia, R.; Ager, J. W.; Guo, J.; Javey, A. *Nano Lett.* **2014**, *14* (8), 4592−7.

(34) Fiori, G.; Bonaccorso, F.; Iannaccone, G.; Palacios, T.; Neumaier, D.; Seabaugh, A.; Banerjee, S. K.; Colombo, L. *Nat. Nanotechnol.* **2014**, *9* (10), 768−79.

(35) Shi, S.-F.; Wang, F. *Nat. Nanotechnol.* **2014**, *9* (9), 664−665.

(36) Schaibley, J.; Xu, X. *Nat. Phys.* **2014**, *10* (11), 798−799.

(37) Niu, T.; Li, A. *Prog. Surf. Sci.* **2015**, *90* (1), 21−45.

(38) Lu, N.; Guo, H.; Li, L.; Dai, J.; Wang, L.; Mei, W. N.; Wu, X.; Zeng, X. C. *Nanoscale* **2014**, *6* (5), 2879−86.

(39) Liu, K.-K.; Zhang, W.; Lee, Y.-H.; Lin, Y.-C.; Chang, M.-T.; Su, C.-Y.; Chang, C.-S.; Li, H.; Shi, Y.; Zhang, H.; Lai, C.-S.; Li, L.-J. *Nano Lett.* **2012**, *12* (3), 1538−1544.

(40) Shi, Y.; Zhou, W.; Lu, A.-Y.; Fang, W.; Lee, Y.-H.; Hsu, A. L.; Kim, S. M.; Kim, K. K.; Yang, H. Y.; Li, L.-J.; Idrobo, J.-C.; Kong, J. *Nano Lett.* **2012**, *12* (6), 2784−2791.

(41) Sørensen, S. G.; Füchtbauer, H. G.; Tuxen, A. K.; Walton, A. S.; Lauritsen, J. V. *ACS Nano* **2014**, *8* (7), 6788−6796.

(42) Shaw, J.; Zhou, H.; Chen, Y.; Weiss, N.; Liu, Y.; Huang, Y.; Duan, X. *Nano Res.* **2014**, *7* (4), 511−517.

(43) Huang, C.; Wu, S.; Sanchez, A. M.; Peters, J. J.; Beanland, R.; Ross, J. S.; Rivera, P.; Yao, W.; Cobden, D. H.; Xu, X. *Nat. Mater.* **2014**, *13* (12), 1096−101.

(44) Yuan, H.; Bahramy, M. S.; Morimoto, K.; Wu, S.; Nomura, K.; Yang, B.-J.; Shimotani, H.; Suzuki, R.; Toh, M.; Kloc, C.; Xu, X.; Arita, R.; Nagaosa, N.; Iwasa, Y. *Nat. Phys.* **2013**, *9* (9), 563−569.

(45) Komesu, T.; Le, D.; Zhang, X.; Ma, Q.; Schwier, E. F.; Kojima, Y.; Zheng, M.; Iwasawa, H.; Shimada, K.; Taniguchi, M.; Bartels, L.; Rahman, T. S.; Dowben, P. A. *Appl. Phys. Lett.* **2014**, *105* (24), 241602.

(46) Ross, J. S.; Klement, P.; Jones, A. M.; Ghimire, N. J.; Yan, J.; Mandrus, D. G.; Taniguchi, T.; Watanabe, K.; Kitamura, K.; Yao, W.; Cobden, D. H.; Xu, X. *Nat. Nanotechnol.* **2014**, *9* (4), 268−72.

(47) Kane, C. L.; Mele, E. J. *Phys. Rev. Lett.* **2005**, *95* (22), 226801.

(48) Lee, D.; Riedl, C.; Beringer, T.; Castro Neto, A.; von Klitzing, K.; Starke, U.; Smet, J. *Phys. Rev. Lett.* **2011**, *107* (21), 216602.

(49) Abanin, D. A.; Pesin, D. A. *Phys. Rev. Lett.* **2012**, *109* (6), 066802.

(50) Subramaniam, D.; Libisch, F.; Li, Y.; Pauly, C.; Geringer, V.; Reiter, R.; Mashoff, T.; Liebmann, M.; Burgdörfer, J.; Busse, C.; Michely, T.; Mazzarello, R.; Pratzer, M.; Morgenstern, M. *Phys. Rev. Lett.* **2012**, *108*, 046801.

(51) Han, W.; Kawakami, R. K.; Gmitra, M.; Fabian, J. *Nat. Nanotechnol.* **2014**, *9* (10), 794−807.

(52) Xu, X.; Yao, W.; Xiao, D.; Heinz, T. F. *Nat. Phys.* **2014**, *10* (5), 343−350.

(53) Le, D.; Barinov, A.; Preciado, E.; Isarraraz, M.; Tanabe, I.; Komesu, T.; Troha, C.; Bartels, L.; Rahman, T. S.; Dowben, P. A. *J. Phys.: Condens. Matter* **2015**, *27* (18), 182201.

(54) Song, C.-L.; Wang, Y.-L.; Jiang, Y.-P.; Zhang, Y.; Chang, C.-Z.; Wang, L.; He, K.; Chen, X.; Jia, J.-F.; Wang, Y.; Fang, Z.; Dai, X.; Xie, X.-C.; Qi, X.-L.; Zhang, S.-C.; Xue, Q.-K.; Ma, X. *Appl. Phys. Lett.* **2010**, *97* (14), 143118.

(55) Wang, Q.; Zhang, W.; Wang, L.; He, K.; Ma, X.; Xue, Q. *J. Phys.: Condens. Matter* **2013**, *25* (9), 095002.

(56) Kim, Y. K.; Krupin, O.; Denlinger, J. D.; Bostwick, A.; Rotenberg, E.; Zhao, Q.; Mitchell, J. F.; Allen, J. W.; Kim, B. J. *Science* **2014**, *345* (6193), 187−190.

(57) Bradley, A. J.; M. Ugeda, M.; da Jornada, F. H.; Qiu, D. Y.; Ruan, W.; Zhang, Y.; Wickenburg, S.; Riss, A.; Lu, J.; Mo, S.-K.; Hussain, Z.; Shen, Z.-X.; Louie, S. G.; Crommie, M. F. *Nano Lett.* **2015**, *15* (4), 2594−2599.

(58) Tan, S.; Zhang, Y.; Xia, M.; Ye, Z.; Chen, F.; Xie, X.; Peng, R.; Xu, D.; Fan, Q.; Xu, H.; Jiang, J.; Zhang, T.; Lai, X.; Xiang, T.; Hu, J.; Xie, B.; Feng, D. *Nat. Mater.* **2013**, *12* (7), 634−40.

(59) He, K.; Kumar, N.; Zhao, L.; Wang, Z.; Mak, K. F.; Zhao, H.; Shan, J. *Phys. Rev. Lett.* **2014**, *113* (2), 026803.

(60) Wang, G.; Marie, X.; Gerber, I.; Amand, T.; Lagarde, D.; Bouet, L.; Vidal, M.; Balocchi, A.; Urbaszek, B. *Phys. Rev. Lett.* **2015**, *114* (9), 097403.